ACS APPLIED POLYMER MATERIALS

pubs.acs.org/acsapm
Article

Substituents and Resonance Effects on the Electrochemical Stability of Polyelectrochromic Triarylamine-Based Polymers

Yaw-Terng Chern,* Shu-Juan Zhang, Shao-Jung Ho, Yu-Jen Shao, Yu-Jie Wang, and Guey-Sheng Liou*

Cite This: https://doi.org/10.1021/acsapm.4c00432

ABSTRACT: Two polyamides (PAs) (**PA1** and **PA2**) with three electroactive nitrogen atoms within triphenylamine (TPA)-containing structures were synthesized from two diamine monomers, 4,4′--bis[(2,4-dimethoxyphenyl)(4-aminophenyl)-amino]-2″,4′′-dimethoxytriphenylamine (**1-NH$_2$**) or 4,4′-bis(4-aminophenyl(4-methylphenyl)amino)-4′-methyltriphenylamine (**2-NH$_2$**), and dicarboxylic acids via a phosphorylation polyamidation technique. **PA1** exhibited highly integrated electrochromic performances, including multiple color changes (colorless to grass green, green, and blue), fast response speed (7.7/2.6 s at 422 nm for the first electrochromic process), high contrast of optical transmittance change (ΔT = 54% at 422 nm at the first oxidation stage), and excellent electrochromic stability. Introducing electron-donating *ortho* and *para* methoxy substituents and three electroactive nitrogen centers could effectively increase the electrochromic stability of the resulting **PA1**. At the first oxidation stage, **PA1** exhibited the highest electrochromic stability (only 4.1 and 2.5% decay of its coloration efficiency (CE) at 422 and 1252 nm after 15,000 switching cycles, respectively) compared to all other TPA-based polymers. It was noteworthy for the first time that the polymers containing more electroactive nitrogen centers reveal longer wavelength absorption in the near-infrared (NIR) region at the first oxidation stage due to cation radical delocalization. The delocalization could facilitate electrochromic stability, and the relationship between the structures and electrochromic stability for these TPA-based polymers was also investigated. In addition, these PAs exhibited good solubility in many solvents and could be solution-cast into flexible films. They showed good thermal stability with glass transition temperatures ranging from 236 to 278 °C and 10% weight loss in nitrogen at temperatures above 425 °C.

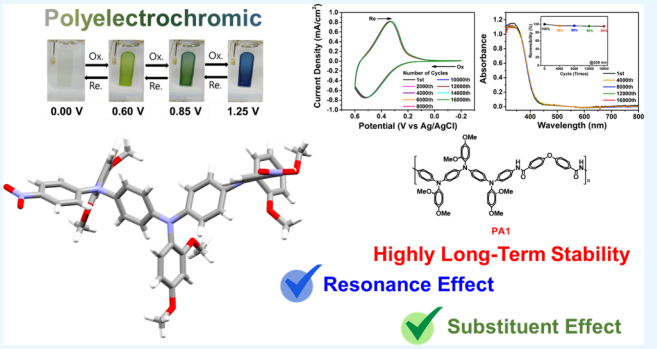

KEYWORDS: *triarylamine, polyelectrochromic, highly stable, substitution effect, resonance effect*

1. INTRODUCTION

Electrochromism is a fascinating phenomenon in materials science and optics that involves reversible changes in color or optical properties upon electrochemically oxidizing or reducing materials.[1,2] They have attracted significant attention and have been studied extensively for various applications, including smart windows, antiglazing mirrors, and electrochromic (EC) displays.[3−6] EC materials can be classified into organic and inorganic categories. The first observation and study in EC materials began with inorganic compounds such as Prussian blue and tungsten trioxide (WO_3).[7] However, inorganic EC materials are limited in manifesting diverse colors and coloring adjustments. Organic materials such as conducting polymers and viologens have recently become an intensive research topic.[8−13] The conducting polymers have several advantages over inorganic compounds as EC materials, including good electrochemical stability, fast switching speed, high coloring efficiency (CE), easy large-area processing, and color tuning through chemical modification. Also, triphenylamine (TPA)-containing polymers have been developed as an attractive family of EC materials because of their colorless neutral state and intriguing EC behaviors.[14−22] In recent years, redox-active materials with optical absorption change in the near IR (NIR) region have drawn significant attention due to their potential applications in optical communication, data storage, and thermal control in buildings and spacecraft.[5,23−29] For example, Wan et al. reported that the quinone-containing EC materials revealed high absorption in NIR upon electrochemical reduction.[30] Reynolds and Beaujuge reported that the conjugated polymers could exhibit multicolor in the neutral state and transmission in the oxidized state.[31,32] Liou and Lin also noted that the TPA-based polymers demonstrated an attractive anodic EC system for NIR applications due to their

Received: February 9, 2024
Revised: April 17, 2024
Accepted: April 22, 2024

particular intramolecular electron transfer in the oxidized forms.[15]

In 1967, Robin and Day stated that the *N*,*N*,*N*′,*N*′-tetraphenyl-*p*-phenylenediamine (TPPA) cation radical could behave as a symmetrical delocalized class III structure with strong electronic coupling (the electron could delocalize over the two redox centers).[33] Nelson and Adams reported that the unsubstituted TPA moieties undergo dimerization to tetraphenylbenzidine after the formation of a cation radical.[34,35] When electron-donating substituents incorporated the phenyl groups at the para-position of TPA, the dimerization could be effectively reduced by affording stable cationic radicals.[36,37] Although the influence of the substituents on the EC stability of materials has been mentioned, the structure/electrochromic stability relationships for TPA-based polymers are still unclear.

Some critical issues for EC materials, such as electrochemical stability, rapid switching speed, high CE, and high optical transmittance change ($\Delta T\%$) during operation, play essential roles. Among the above characteristics, the EC stability of the polymers is crucially vital to the practical use of materials for any purpose.[38] TPA-based EC materials have been developed for decades and usually have limited electrochemical stability. Most TPA-based polymers revealed their optical reversibility at 90% after only 2000 switching cycles.[20,39,40] However, TPA-based polyamides (PAs) derived from two specific diamines demonstrated significantly enhanced EC stability, with their electroactivity decaying less than 10% even after 10,000 switching cycles.[14,16] As a result, achieving advanced EC stability for TPA-based polymers remains a challenging task, and research in the future is inevitable to address this issue more intensively.

This research aims to develop organosoluble PAs with outstanding EC stability, fast switching speed, high CE, and multiple coloring changes, especially for further enhancing the EC stability. This study provides strategies, including the introduction of numerous redox-active nitrogen centers and electron-donating methoxy substituents. Therefore, we focus on explicitly designing TPA-based PAs containing ortho- and para-substituted methoxy groups and three electroactive nitrogen centers within four phenyl rings. The physical properties, such as thermal stability and electrochemical and spectroelectrochemical stability, were investigated. Furthermore, we also elucidated the effects of the substituents and the number of electroactive nitrogen centers within triarylamine moieties on the EC stability of PAs. This work aimed to obtain more fundamental information on the relationships between cation radical stability and the EC stability of the resulting polymers and compare it with previous reports on the structure-related TPA-based polyamides, such as **PA1′** and **PA3**.[14,15]

2. EXPERIMENTAL SECTION

2.1. Materials. For dehydration, we added CaH_2 into *N*-methyl-2-pyrrolidone (NMP) and dimethyl sulfoxide (DMSO) and then distilled them in vacuo before use. $CaCl_2$ subjected to high-temperature vacuum drying was added to acetonitrile for water removal. The dry 4 Å molecular sieves were added to pyridine and triphenyl phosphite (TPP) for water removal. Tetrabutylammonium perchlorate (TBAP) was recrystallized with ethyl acetate and dried in vacuo before use. **PA1′**, **PA3**, 4,4′-bis[(4-nitrophenyl)amino]-diphenylamine, and 9,9-bis[4-(4-carboxy-phenoxy)phenyl]fluorene were synthesized according to a previous method.[14,15,41,42] All other reagents were used as received from commercial sources.

2.2. Synthesis of 4,4′-Bis[(2,4-dimethoxyphenyl)(4-nitrophenyl)amino]-2″,4″′-dimethoxytriphenylamine (1-NO_2). In a 150 mL three-neck flask, 5 g (11.3 mmol) of 4,4′-bis[(4-nitrophenyl)amino]diphenylamine, 11.2 g (42.4 mmol) of 1-iodo-2,4-dimethoxybenzene, 2.7 g of copper powder, 5.87 g of K_2CO_3, 3.5 g of 18-crown-6-ether, and 16 mL of *o*-dichlorobenzene were added. The reaction mixture was refluxed under a nitrogen atmosphere for 24 h. Afterward, while the reaction mixture was still hot, the copper powder was filtered out, and the filtrate was cooled to undergo recrystallization. The product was collected to yield 2.5 g (71%) of yellow crystal: mp 192−194 °C. IR (KBr): 3037 (ar. C−H str.), 2940, 2837 (al. C−H str.), 1589 (sym. NO_2 str.), 1303 (asym. NO_2 str.). ^{1}H NMR (600 MHz, $CDCl_3$, ppm): 3.68 (s, 3H), 3.71 (s, 6H), 3.83 (ss, 9H), 6.51 (m, 3H), 6.52 (m, 3H) 6.28 (d, J = 9.6 Hz, 4H), 6.96 (d, J = 9.0 Hz, 4H), 7.09 (d, J = 9.0 Hz, 4H), 7.13 (m, 3H), 7.97 (d, J = 9.6 Hz, 4H). ^{13}C NMR (150 MHz, $CDCl_3$, ppm): 55.55, 55.58, 55.66, 55.72, 100.38, 100.70, 105.50, 114.09, 121.85, 125.70, 126.32, 127.19, 127.75, 130.90, 131.32, 138.22, 138.64, 145.57, 154.49, 156.89, 157.44, 159.62, 160.26. HRMS (m/z), [M+H$^+$] calculated: 850.3083, found: 850.3065. Crystal data: $C_{48}H_{43}N_5O_{10}$, crystal of 0.58 × 0.18 × 0.04 mm, triclinic with a = 11.749 (5) Å, b = 12.554 (5) Å, c = 17.253 (5) Å, α = 74.340 (5)°, β = 74.891 (5)°, γ = 87.680 (5)° with Dc = 1.194 Mg/m^3 for Z = 2, V = 2364.4 (15) Å^3, T = 200 K, λ = 0.71073 Å, F(000) = 892, final R indices: R1 = 0.0807, WR2 = 0.1968.

2.3. Synthesis of 4,4′-Bis[4-methylphenyl(4-nitrophenyl)-amino]-4″-methyltriphenylamine (2-NO_2). A 150 mL three-neck flask was charged with 4 g (9.07 mmol) of 4,4′-bis[(4-nitrophenyl)-amino]diphenylamine, 7.1 g (32.6 mmol) of 4-iodotoluene, 2.1 g of copper powder, 4.5 g of K_2CO_3, 3.0 g of 18-crown-6-ether, and 20 mL of *o*-dichlorobenzene. The mixture was heated to reflux under a nitrogen atmosphere for 24 h. The mixture was then filtered to remove the copper powder, and the filtrate was allowed to cool, resulting in the precipitation of the red crude product. The product was purified and dried and then was collected to yield 5.2 g (80%) of red powder: mp 306-310 °C. IR (KBr): 3024 (ar. C−H str.), 2964, 2862 (al. C−H str.), 1588 (sym. NO_2 str.), 1317 (asym. NO_2 str.). ^{1}H NMR (600 MHz, $CDCl_3$, ppm): 2.33 (s, 3H), 2.36 (s, 6H), 6.86 (d, J = 9.6 Hz, 4H), 7.04 (2s, 8H), 7.06 (d, J = 8.4 Hz, 2H), 7.10 (d, J = 8.4 Hz, 4H), 7.13 (d, J = 8.4 Hz, 2H), 7.19 (d, J = 8.4 Hz, 4H), 8.01 (d, J = 9.6 Hz, 4H). ^{13}C NMR (150 MHz, $CDCl_3$, δ, ppm): 20.90, 21.01, 116.95, 124.22, 125.51, 126.66, 127.33, 130.27, 130.54, 130.63, 133.92, 135.93, 139.55, 139.65, 142.84, 144.38, 145.29, 153.69. HRMS (m/z), [M$^+$] calculated: 711.2840, found: 711.2839.

2.4. Synthesis of 4,4′-Bis[(2,4-dimethoxyphenyl)(4-aminophenyl)amino]-2″,4″′-dimethoxytriphenylamine (1-NH_2). In a 250 mL three-neck flask, 15 g (17.7 mmol) of **2**, 1.2 g of Pd/C, and 50 mL of DMF were added, and the mixture was stirred under a hydrogen atmosphere at room temperature until the theoretical amount of hydrogen was consumed. The time to reach this stage is about 48 h. Afterward, Pd/C was filtered out, and the filtrate was precipitated into methanol. The product was collected to yield 9.6 g (83%) of pale purple powder: mp 195−197 °C. IR (KBr): 3454, 3371(N−H str.), 3034 (ar. C−H str.), 2937, 2835 (al. C−H str.) ^{1}H NMR (500 MHz, DMSO-d_6, δ, ppm): 3.63 (9H), 3.74 (9H), 4.78 (s, 4H), 6.40 (d, J = 9.0 Hz, 4H), 6.49 (m, 7H), 6.57 (d, J = 9.0 Hz, 4H), 6.60 (m, 3H), 6.73 (d, J = 8.5 Hz, 4H), 7.00 (m, 3H).^{13}C NMR (125 MHz, DMSO-d_6, δ, ppm): 55.26, 55.59, 55.63, 100.23, 100.31, 105.54, 105.61, 114.61, 117.60, 120.99, 124.97, 128.31, 128.46, 130.45, 130.60, 136.56, 139.80, 142.87, 144.30, 156.75, 156.85, 158.09, 158.17. HRMS (m/z), [M$^+$] calculated: 789.3521, found: 789.3505.

2.5. Synthesis of 4,4′-Bis[4-methylphenyl(4-aminophenyl)-amino]-4″-methyltriphenylamine (2-NH_2). The synthesis procedure of **2-NH_2** was the same as that of **1-NH_2**, and its ^{1}H and ^{13}C NMR spectra were characterized and are shown in Figure S8. IR (KBr): 3442, 3359(N−H str.), 3031 (ar. C−H str.), 2916, 2857 (al. C−H str.) HRMS (m/z), [M$^+$] calculated: 651.3356, found: 651.3348.

2.6. Polymer Synthesis. Using the synthesis of **PA1** as an example and the synthetic route illustrated in Scheme S1, in a 100 mL

https://doi.org/10.1021/acsapm.4c00432
ACS Appl. Polym. Mater. XXXX, XXX, XXX−XXX

Scheme 1. Synthesis of Compounds 1-NO_2, 2-NO_2, 1-NH_2, and 2-NH_2

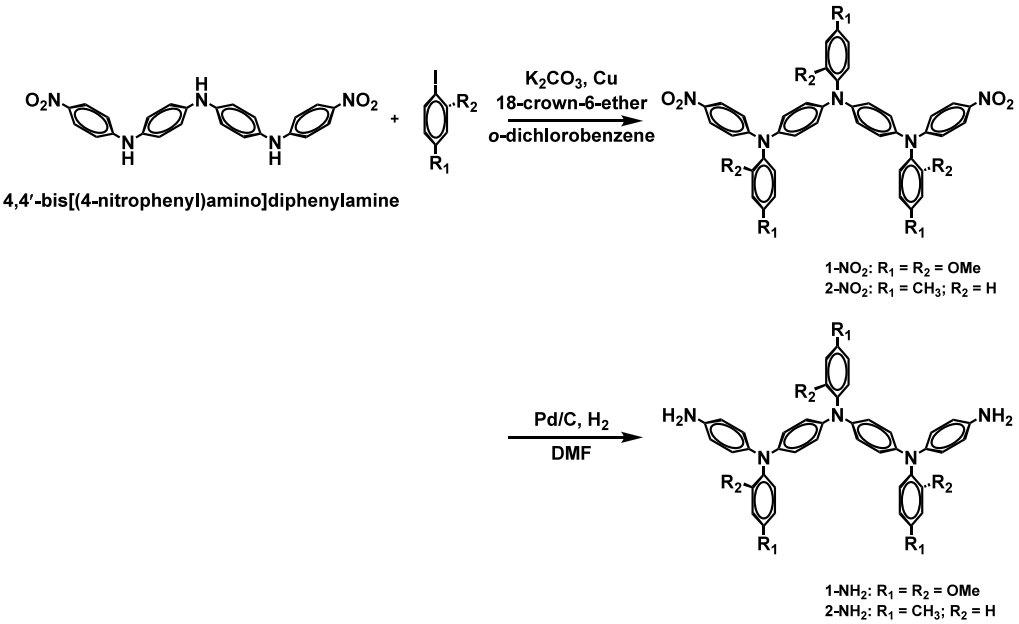

three-neck flask, 1.594 g (2 mmol) of monomer **1-NH_2**, 0.516 g (2 mmol) of 4,4′-dicarboxydiphenyl ether, 2.5 mL of NMP, 2.0 mL of TPP, 0.7 mL of pyridine, and 0.2 g of $CaCl_2$ were added. The reaction was conducted at 120 °C under a nitrogen atmosphere for 6 h. The obtained polymer solution was poured into 250 mL of stirred methanol, forming stringy and fiber-like precipitation, washed several times with hot water, and then vacuum-dried. The obtained **PA1** was dissolved in DMAc, and the solution was precipitated again in methanol for purification. The inherent viscosity of purified **PA1** was measured to be 0.49 dL/g using NMP as the solvent. IR(KBr): 1655 (C=O), 3444 cm^{-1} (N−H str.). ^1H NMR (500 MHz, DMSO-d_6, δ, ppm): 3.65 (9H), 3.76 (9H), 6.53−6.74 (m, 14H), 6.80 (d, J = 8.5 Hz, 4H), 7.08 (m, 7H), 7.50 (d, J = 8.5 Hz, 4H), 8.00 (d, J = 8.5 Hz, 4H), 10.03 (s, 2H).

2.7. Electrochemical and Spectroelectrochemical Characterization. Electrochemical property characterization, including cyclic voltammetry (CV) and electrochemical impedance spectroscopy (EIS), was conducted through a CH Instruments 6122E Electrochemical Analyzer. The electrochemical analyzer used a three-electrode system containing a platinum counter electrode, a polymer film coated on ITO glass (0.6 cm × 3 cm) as working electrode, and a Ag/AgCl reference electrode in 30 mL anhydrous acetonitrile with 0.1 M $TBABF_4$ as a supporting electrolyte under an air atmosphere. The testing frequency of EIS was from 1.0 MHz to 0.1 Hz. The absorbance spectrum of spectroelectrochemistry and switching time was recorded on an Agilent UV−vis spectrophotometer.

3. RESULTS AND DISCUSSION

3.1. Monomer Synthesis. Two diamines 4,4′-bis[4-aminophenyl(2,4-dimethoxyphenyl)amino]-2″,4′′-dimethoxytriphenylamine (**1-NH_2**) and 4,4′-bis[4-aminophenyl(4-methylphenyl)amino]-4″-methyltriphenylamine (**2-NH_2**) were synthesized from 4,4′-bis[(4-nitrophenyl)amino]-diphenylamine, as shown in Scheme 1. The C−N coupling was performed by reactions of 4,4′-bis[(4-nitrophenyl)amino]-diphenylamine with 1-iodo-2,4-dimethoxybenzene and 4-iodotoluene in the presence of copper to afford compounds **1-NO_2** and **2-NO_2**, respectively. Subsequently, hydrogenation was followed to yield diamine monomers **1-NH_2** and **2-NH_2**. IR and NMR spectroscopic techniques were used to identify the structures of the intermediate compounds (**1-NO_2** and **2-NO_2**) and the target diamine monomers (**1-NH_2** and **2-NH_2**). The FTIR spectra of the obtained compounds are depicted in the Supporting Information in Figures S1 and S2. Compounds **1-NO_2** and **2-NO_2** exhibited two characteristic bands at around 1589/1303 and 1588/1317 cm^{-1} due to the nitro asymmetric and symmetric stretching. After reduction to diamine monomers **1-NH_2** and **2-NH_2**, the characteristic absorption bands of the nitro group disappeared, and the primary amino group characteristic bands appeared at 3454/3371 and 3442/3359 cm^{-1} (N−H stretching), respectively. The ^1H and ^{13}C NMR spectra of monomers are illustrated in Figure 1 and Figures S3−S10 and agree well with the proposed molecular structures. The signals at 4.78 and 5.61 ppm are assigned to the amino groups of monomers **1-NH_2** and **2-NH_2**, respectively (Figures S7a and S8a). In addition, dinitro compound **1-NO_2** was confirmed by X-ray crystal analysis from the single crystal obtained by slow crystallization from DMF. As shown in Figure 2, **1-NO_2** displays a propeller-shaped configuration of the TPA core, and these seven phenyl rings are not in the same plane. Its shortest distance of face-to-face $\pi-\pi$ interaction is 5.912 Å, demonstrating that the whole structure is a twisted conformation.

3.2. Polymer Synthesis and Basic Properties. According to the phosphorylation method described by Yamazaki et al.,[43,44] polyamides **PA1** and **PA2** were synthesized from the diamine monomers **1-NH_2** and **2-NH_2**, respectively, with aromatic dicarboxylic acids (Scheme S1). Furthermore, **PA1′** and **PA3**, as shown in Figure 2c, were also prepared to compare the electrochemical and electrochromic properties. All polymerization reactions proceeded homogeneously and yielded high inherent viscosities. The obtained **PA1** and **PA2** revealed inherent viscosities of 0.49 and 0.42 dL/g (Table S1), respectively, and all of the polymers could afford transparent and flexible films via solution casting. IR and ^1H NMR spectroscopy confirmed the formation of PAs. A typical IR spectrum of **PA1** exhibited characteristic absorption bands of the amide group at around 3444 cm^{-1} (N−H stretch) and 1655 cm^{-1} (amide carbonyl) (Figure S2). Additionally, the NMR spectrum also confirmed the chemical structure of **PA1**,

https://doi.org/10.1021/acsapm.4c00432
ACS Appl. Polym. Mater. XXXX, XXX, XXX−XXX

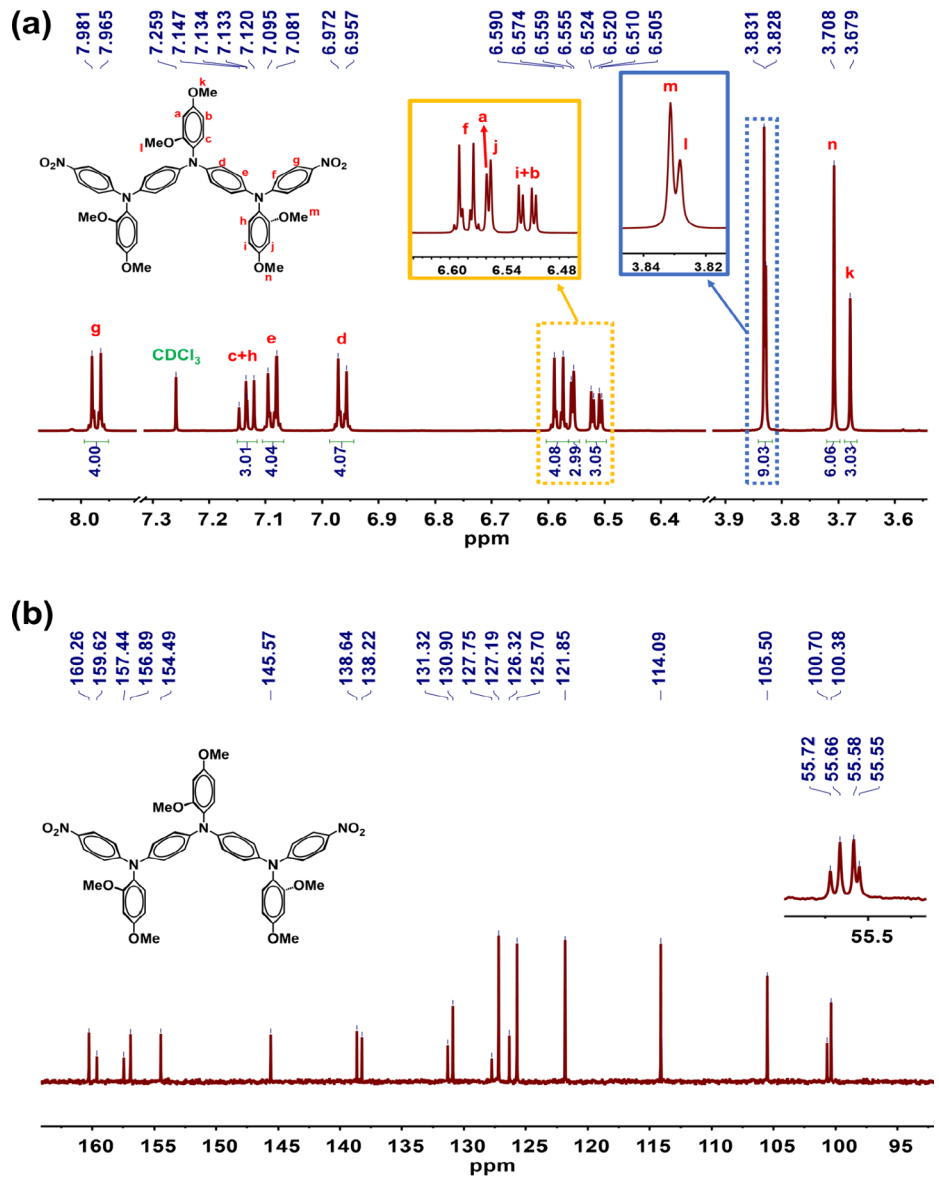

Figure 1. (a) ^{1}H and (b) ^{13}C NMR spectra of **1-NO$_2$** ($CDCl_3$).

and the assignment of protons for **PA1** is depicted in Figure S13.

The solubilities of PAs (PAs) were tested in various solvents, and the solubility data are summarized in Table S1. **PA1** exhibited a much higher solubility than **PA2** in the different solvents, and all PAs were soluble in NMP and *o*-chlorophenol. The superb solubility of **PA1** could be ascribed to the packing-disruptive 2,4-dimethoxyphenyl pendant groups, which increase chain packing distances and decrease the intermolecular interaction. The excellent solubility makes **PA1** a potential candidate for practical applications through spin-coating or inkjet-printing processes to produce thin films for optoelectronic devices. Although dicarboxylic acid, with a kink and a bulky unit, was introduced into the polymer structure of **PA2**, the resulting polyamide exhibited poor solubility. It was only soluble in NMP and *o*-chlorophenol. In contrast, **PA1** demonstrated higher solubility than **PA2**, suggesting that incorporating 2,4-dimethoxyphenyl groups into the polymer chain could enhance the solubility.

Thermal analysis was conducted using DSC, TMA, and TGA, and the obtained thermal properties are summarized in Table S2. Typical TGA and TMA curves of the representative polymers **PA1** and **PA2** are depicted in Figures S14 and S15. Dynamic thermogravimetry revealed relatively good thermal stability of the prepared polyamides. Typical TGA curves of **PA1** and **PA2** in air and nitrogen atmospheres exhibited good thermal stability with insignificant weight loss up to 400 °C. The mechanical relaxation spectra of **PA1** and **PA2** are illustrated in Figures S16 and S17, respectively. Based on the tan δ and E'' peaks, the glass transition temperatures of **PA1** and **PA2** were observed at 236 and 269 °C, respectively. In addition, the softening temperatures (T_s) of the polymer films were determined from the onset temperature of the probe displacement on the TMA trace. Typical TMA curves of representative **PA1** and **PA2** are depicted as insets in Figures S14 and S15, and the T_s is observed at 199 and 217 °C for **PA1** and **PA2**, respectively.

3.3. Electrochemical Properties. The electrochemical behaviors of the PAs were investigated by using cyclic

https://doi.org/10.1021/acsapm.4c00432
ACS Appl. Polym. Mater. XXXX, XXX, XXX−XXX

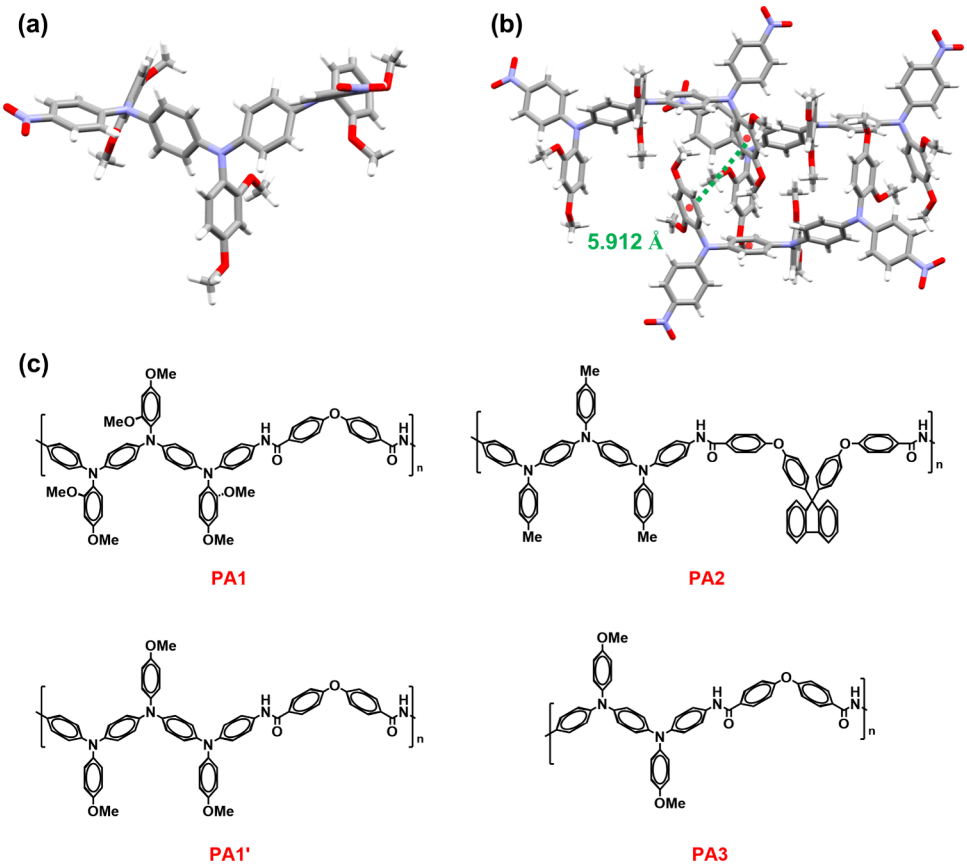

Figure 2. (a) Single-crystal structure of **1-NO$_2$** and (b) its packing structure. (c) Chemical structures of the studied triarylamine-based polyamides.

voltammetry (CV) measurements, with the polymer film on an ITO as the working electrode and 0.1 M TBAP in anhydrous acetonitrile as the supporting electrolyte. The typical CV diagrams of PAs **PA1** and **PA2** exhibited three quasi-reversible redox couples, corresponding to successive removal of electrons from three different redox-active nitrogen centers (Figure 3a and Figure S18). The electrochemical properties of polymers **PA1** and **PA2** are summarized in Table 1. The first electron removal occurred at the middle nitrogen atom of the three electroactive nitrogen centers because of the highest electron density among all the other nitrogen atoms.[15,45] The CV scans of **PA2** from −0.20 to 0.65 V (Figure 3d) revealed a moderately stable redox process over 6000 cycles, slightly reducing the peak current.

In contrast, the CV scans of **PA1** (Figure 3b), from −0.20 to 0.60 V, demonstrate unprecedented redox stability in continuous 16,000 cycles without a noticeable decrease in the peak current. The first redox process exhibits a transcendent electrochemical stability that might be ascribed to the lower applied potential and resonance stabilization of the resulting cationic radicals, as depicted in Figure 4a. Besides, **PA1′** (Figure S19) and **PA1** revealed a much higher electrochemical stability than **PA2** due to the chemical structures of **PA1′** and **PA1**, containing para methoxy or ortho and para two methoxy substituents, whereas **PA2** only has one para methyl substituent. Furthermore, **PA1** manifested exceptional reversibility according to the characteristic absorption peak of the initial neutral state at 336 nm observed in the UV−vis spectra, as depicted in Figure 3d. Moreover, substituent groups with unshared electron pairs, like methoxy adjacent to the phenyl ring, are more substantial electron-donating groups than ones without unshared electron pairs, like methyl. As a result, the impedance spectroscopy revealed that **PA1** with more methoxy substituents showed a relatively low R_{ct} value (38.3 Ω) than **PA1′** (41.2 Ω). Because of more resonance sites in **PA1** and **PA1′**, the R_{ct} value could persist without an apparent change. Also, **PA1** exhibits a much better electrochemical stability than **PA2**, suggesting that the electron-donating effect of the substituent plays a critical role in the electrochemical stability. For comparison, **PA3** was also measured by CV, as shown in Figure S20a, and exhibited remarkable stable characteristics after 12,000 at the first oxidation stage. However, **PA3** showed apparent current reduction after 2,000 cycles, following the continued decay shown in Figure S20b when applied further to the second oxidation stage.

In contrast, **PA1** and **PA1′** could maintain excellent reversibility up to 8000 cycles to the second oxidation stage, as shown in Figure 3c and Figure S19c, implying that the resonance pathways for dicationic radicals are critical for the materials preserving highly stable behaviors. During the electrochemical oxidation of the PAs, the color of polymer film **PA2** changed from colorless to yellow-green, purple, and blue (Figure S21). In contrast, the color of polymer film **PA1** changed from colorless to grass green, green, and blue (Figure 5), implying that altering the substituents attached to the phenyl ring can achieve a color-tuning effect. According to the optical properties and redox potentials of **PA1** and **PA2**, their respective highest occupied molecular orbital (HOMO) and lowest unoccupied molecular orbital (LUMO) (versus vacuum) were calculated and are summarized in Table S3. The HOMO level of polymers **PA1** and **PA2** could be

https://doi.org/10.1021/acsapm.4c00432
ACS Appl. Polym. Mater. XXXX, XXX, XXX−XXX

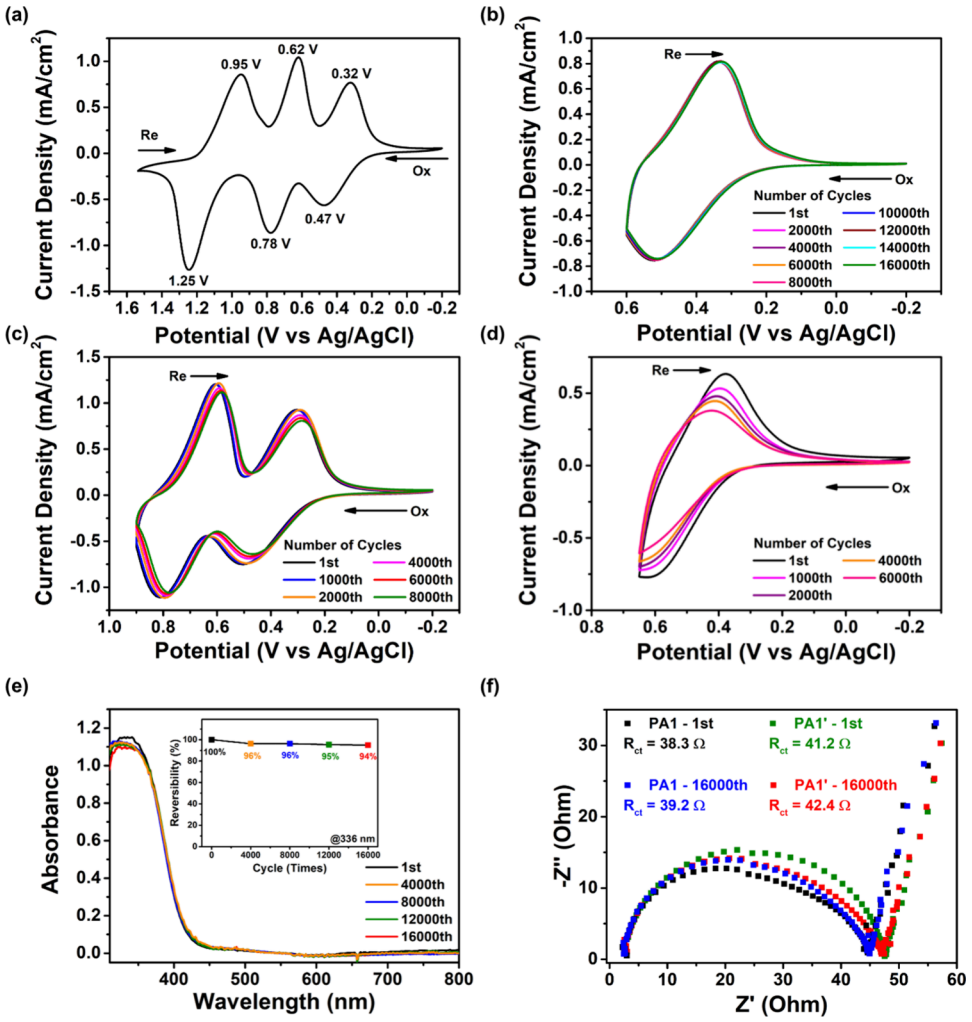

Figure 3. Cyclic voltammetric diagram of the **PA1** film (thickness: 180 ± 10 nm) at a scan rate of 50 mV/s (a) from −0.20 to 1.55 V and its cyclic stabilities at (b) first oxidation stage (−0.20 to 0.60 V) for 16,000 cycles and (c) second oxidation stage (−0.20 to 0.90 V) for 8000 cycles in 0.1 M TBAP/MeCN. (d) Cyclic voltammetric stability diagram of the **PA2** film (thickness: 180 ± 20 nm) at a scan rate of 50 mV/s at the first oxidation stage (−0.20 to 0.65 V) in 0.1 M TBAP/MeCN. (e) UV−vis spectra of the **PA1** film (thickness: 180 ± 10 nm) at the neutral state after different scanning cycles in 0.1 M TBAP/MeCN. (f) Nyquist plots of electrochemical impedance spectroscopy of **PA1** and **PA1′** at the first cycle and after 16,000 cycles measurements.

Table 1. Long-Term Stability of Polymers

polymer	potential (V)	η (cm²/C)[a]	cycles[b]	T (%)[c]	decay (%)[d]	ref
PA1	0.0 → 0.40	195	15,000	54.0	4.1	this study
PA2	0.0 → 0.55	200	4000	63.4	11.5	this study
PA3	0.0 → 0.70	388	10,000	54.0	4.9	15

[a]Initial coloration efficiency. [b]Times of the cyclic scan by applying the potential step. [c]Initial contrast of optical transmittance at 436 nm for **PA1**, 431 nm for **PA2**, and 433 nm for **PA3**. [d]Decay of coloration efficiency after cyclic scans.

estimated from the $E_{1/2}$ values of their oxidation in CV experiments as 4.75 and 4.90 eV, respectively, matching the trend of the results from density functional theory (DFT) calculations that more effective electron-donating groups in the triarylamine architecture possess lower oxidation potentials.

3.4. Spectroelectrochemical Properties. For the spectroelectrochemical study, the spectra of the polymer films coated on the ITO substrate were collected in situ by a UV−vis spectrophotometer under the controlled potentials of an electrochemical analyzer. The typical spectroelectrochemical spectra of **PA2** are illustrated in Figure S21. In the neutral form (0.00 V), the film exhibited strong absorption at around 350 nm, characteristic of triarylamine, and was almost transparent in the visible region. Upon oxidation (increasing the applied voltage from 0.00 to 0.55 V), the intensity of the absorption peak at 350 nm gradually decreased, while a new peak at 431 nm and a broad band centered around 1310 nm in the NIR region gradually increased in intensity. The absorption spectra change in the visible-light range could be ascribed to the formation of a stable monocation radical (**PA2**$^{+\bullet}$) on the main chain. The electron delocalization over the other two nitrogen centers leads to an intervalence charge-transfer (IV-CT) absorption in the NIR region, which Robin and Day reported that the TPPA cation radical is a symmetrical delocalized class III; the electron could be delocalized over the two redox centers, leading to an IV-CT absorption band in the NIR region.[33] With the potential adjusted to 0.8 V corresponding to **PA2**$^{2+}$, the absorption bands (350 and 431 nm) decreased gradually and the absorption band (shift from 1310 to 1090

https://doi.org/10.1021/acsapm.4c00432
ACS Appl. Polym. Mater. XXXX, XXX, XXX−XXX

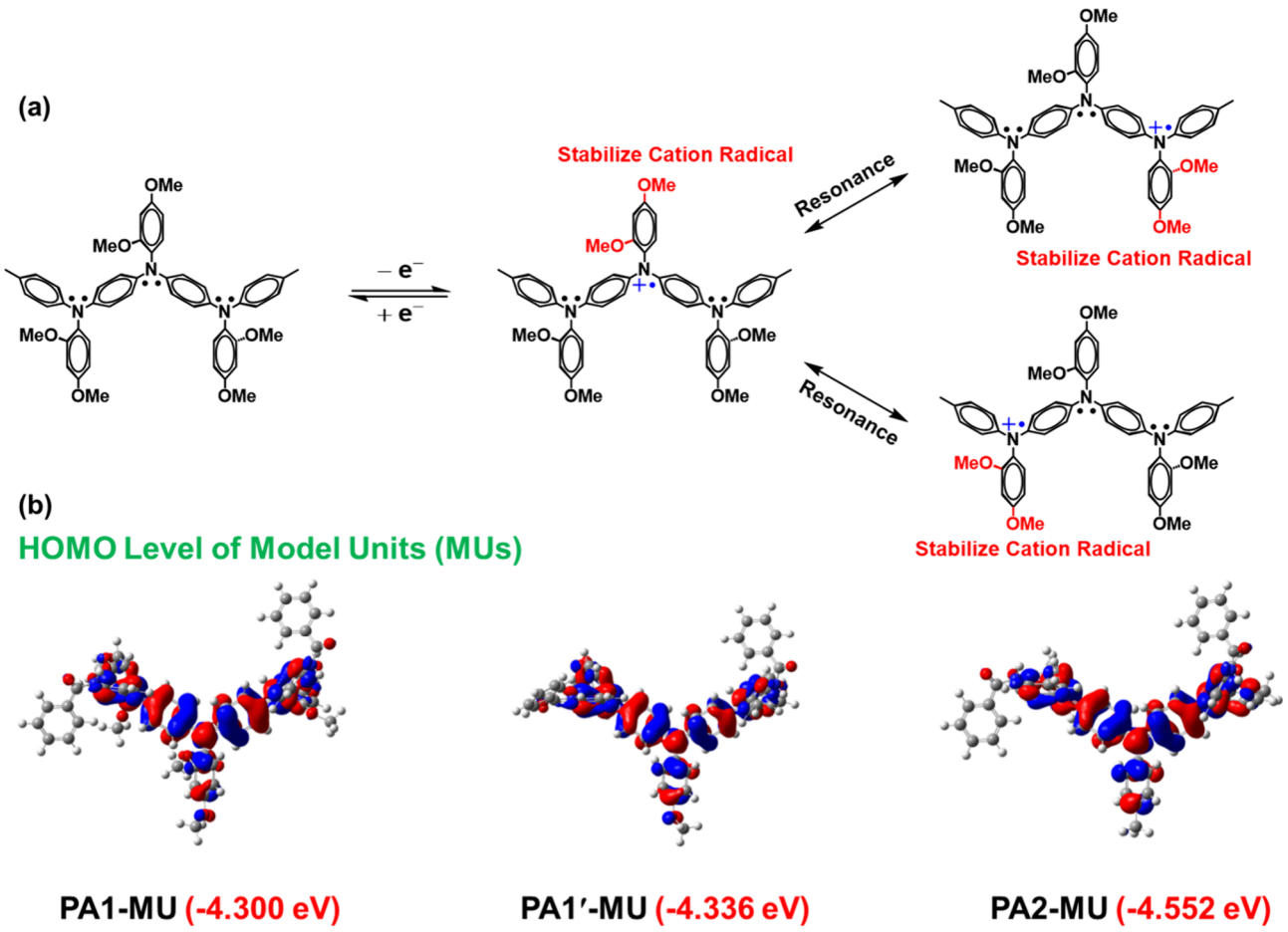

Figure 4. (a) Possible resonance routes of **PA1** at the first oxidation. (b) Calculated highest occupied molecular orbitals of the model units (MUs) of **PA1**, **PA1′**, and **PA2** using density functional theory (DFT) at the B3LYP/6-31G(d) level.

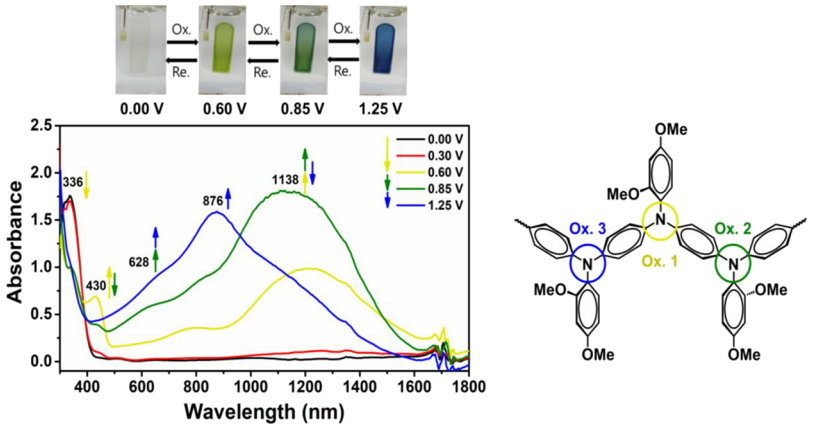

Figure 5. Spectroelectrochemistry of **PA1** (thickness: 330 ± 20 nm) at various applied potentials in 0.1 M TBAP/MeCN.

nm) increased subsequently. When the potential was adjusted to 1.20 V to oxidize the three nitrogen centers completely, the absorption bands at 1090 nm decreased progressively, and the absorption band at 769 nm increased intensively. The disappearance of the NIR absorption band can be attributable to the further oxidation of $\mathbf{PA2}^{2+}$ species to the formation of $\mathbf{PA2}^{3+}$. As depicted in Figure S21, the polymer film changed from colorless in the neutral state to yellow-green for the first oxidation state, purple for the second oxidation state, and blue for the third oxidation state. The polymer **PA2** shows good contrast in the visible and NIR regions, exhibiting high optical transmittance change in the first oxidation stage ($\Delta T\%$) of 63 and 54% at 431 and 1301 nm, respectively, and 93% at 1090 nm in the second oxidation stage.

PA2 and **PA1** revealed different spectroelectrochemical spectra due to the substituent effects. The typical spectroelectrochemical spectra of **PA1** are depicted in Figure 5. In the neutral form (0.00 V), the film exhibited strong absorption at around 350 nm, characteristic of triarylamine, and was nearly transparent in the visible region. Upon oxidation (increasing the applied voltage from 0 to 0.60 V), the intensity of the absorption peak at 336 nm gradually decreased, while a new

https://doi.org/10.1021/acsapm.4c00432
ACS Appl. Polym. Mater. XXXX, XXX, XXX−XXX

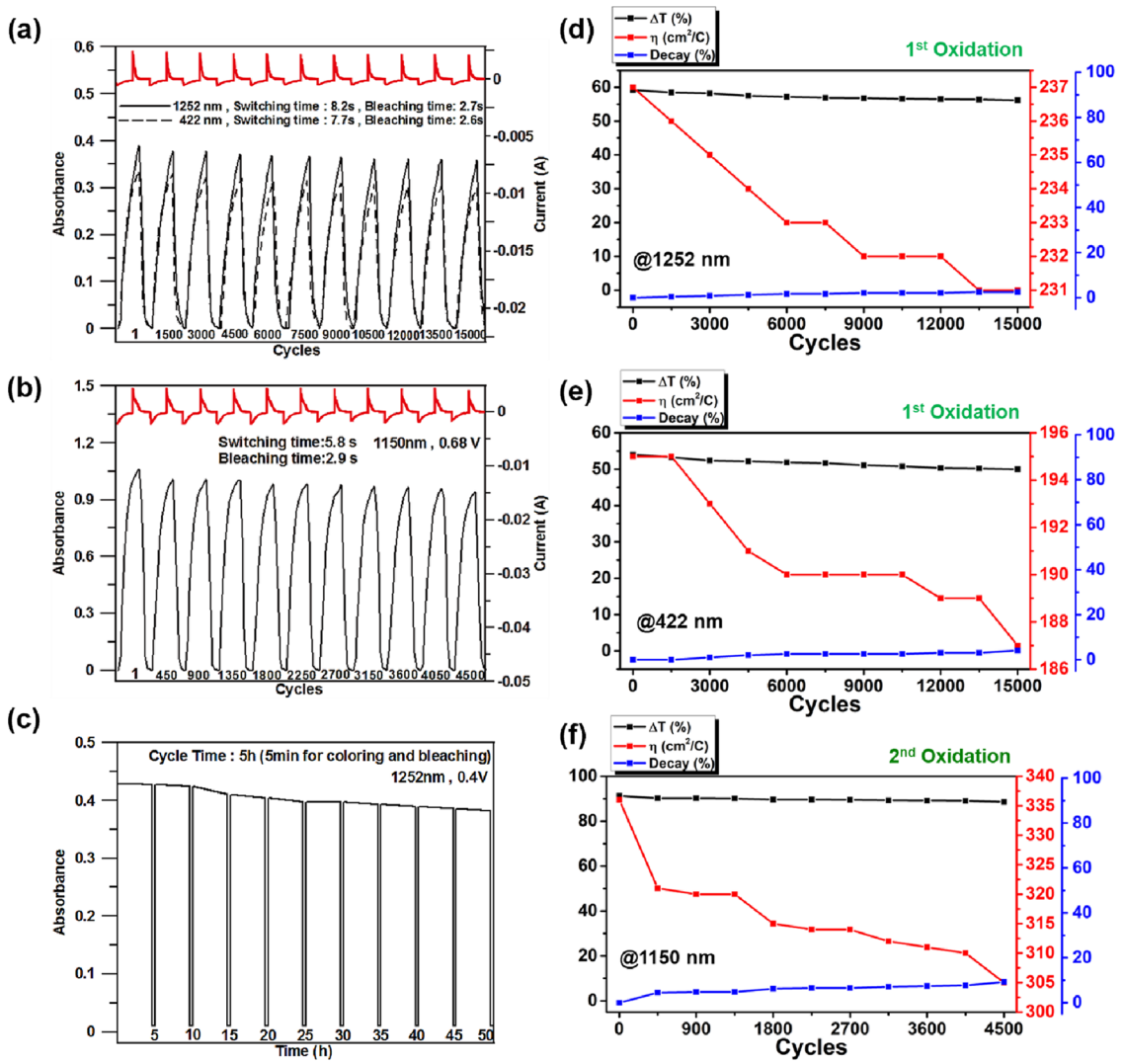

Figure 6. Potential step absorptometry and current consumption of **PA1** (in MeCN with 0.1 M TBAP as the supporting electrolyte) by applying a potential step (a) 0.00 V ↔ 0.40 V and (b) 0.00 V ↔ 0.68 V and cycle time 20 s. (c) Potential step absorptiometry during the continuous cycling test of **PA1** (in MeCN with 0.1 M TBAP as the supporting electrolyte) by switching potentials step 0.00 V ↔ 0.40 V with cycle times of 5 h and 5 min for coloring and bleaching processes, respectively. Plots of ΔT, CE, and the decay percentage of **PA1** for the first oxidation state at (d)1252 and (e) 422 nm and (f) the second oxidation state at 1150 nm and all the results were measured in MeCN with 0.1 M TBAP as the supporting electrolyte.

peak at 430 nm and a broad band centered around 1252 nm in the NIR region gradually increased in intensity. The spectral change in the visible-light range could be attributed to the resulting stable monocation radical ($\mathbf{PA1}^{+\bullet}$). The electron delocalization over the additional two nitrogen centers leads to an IV-CT absorption in the NIR region. With the potential adjusted to 0.85 V corresponding to $\mathbf{PA1}^{2+}$, the absorption bands (336 and 430 nm) decreased gradually, and the absorption band (shift from 1252 to 1138 nm) increased intensively. When the potential was adjusted to 1.25 V to oxidize the three nitrogen centers completely, the absorption bands at 1150 nm decreased obviously and the absorption band (876 nm) increased subsequently. The NIR absorption band disappears because of the further oxidation of $\mathbf{PA1}^{2+}$ species, which leads to the formation of $\mathbf{PA1}^{3+}$. As seen in Figure 5, the appearance of the polymer film changed from colorless in the neutral state to grass green for the first oxidation state, green for the second oxidation state, and blue for the third oxidation state. The polymer **PA1** displayed good contrast in the visible and NIR region, exhibiting high optical transmittance change in the first oxidation stage (ΔT%) of 64 and 83% at 422 and 1252 nm, respectively, and 94% at 1150 nm in the second oxidation stage. The optical change in the transmittance of **PA1** is depicted in Figure S22.

3.5. Electrochromic Switching Properties. The EC switching stability and response time were investigated by monitoring the absorption changes when potential steps were applied in the kinetics studies. Switching data for the representative **PA1** and **PA2** are presented in Figure 6and Figure S23. The electrochromic CE ($\eta = \Delta OD/Q$) and injected charge after various switching cycles were monitored and are summarized in Tables S4−S6. The results for ΔT, CE, and the percentage of CE decay are illustrated in Figure 6d6f. During the first electrochromic switching between 0.0 and 0.55 V, **PA2** exhibited high switching stability and good reversibility, with only 11.5 and 13.5% decay of the CE at 431 and 1301 nm, respectively, in continuous 4000 cycles (Figure S23). The high switching reversibility could be

https://doi.org/10.1021/acsapm.4c00432
ACS Appl. Polym. Mater. XXXX, XXX, XXX−XXX

attributed to the stable redox capability of **PA2** and the excellent adhesion between the polymer film and the ITO substrate. The subsequent section of this review covers a detailed description of the relationship between the chemical structure and switching stability. **PA2** exhibited high CEs of 200 and 238 cm^2/C at 431 and 1301 nm, respectively, for the first EC stage. Additionally, the response time (coloring/bleaching) calculated at 90% of the total optical changes for **PA2** was obtained to be 6.5/1.9 and 4.7/1.7 s at 431 and 1301 nm, respectively, for the first EC process.

In contrast, the first EC switching of **PA1** exhibited a remarkably high switching stability with a much higher reversibility of only 4.10% and 2.53% decay of the CE (195−187 and 237−231 cm^2/C) at 422 and 1252 nm, respectively, in continuous 15,000 cycles (Figure 6a,d,e). This exceptional reversibility can be ascribed to the stable redox property of **PA1** and the excellent adhesion between the polymer film and the ITO substrate. Furthermore, the second stage of EC switching of **PA1** between 0.0 and 0.68 V exhibited high switching stability and good reversibility, with only a 9.2% decay of the CE (336−305 cm^2/C) at 1150 nm in continuous 4500 cycles in Figure 6b,f. The polyamides of **PA2** and **PA1** could switch quickly in the first and second stages. Moreover, another measurement of the long-term stability for **PA1**, maintaining 5 h at each coloring stage with an applied potential of 0.40 V, as illustrated in Figure 6c, confirms that **PA1** could preserve the exceptional long-term EC stability well. Consequently, the designed and synthesized **PA1** exhibits the highest EC switching stability to our knowledge compared with all other TPA-based EC polymers.

3.6. Relationship between the Chemical Structure and Switching Stability. Due to the different number of redox-active centers in these EC polymer chains, the IV-CT absorption band in the NIR region of materials manifests changes during the oxidation process. To confirm the relationships between the NIR absorption band and the number of electroactive nitrogen centers, UV−vis−NIR absorption spectra correlated to applied potentials for **PA1**, **PA1′**, and **PA3** were measured and are illustrated in Figure S24. The λ_{max} and absorption range over the NIR region in the first stage oxidation for **PA1** and **PA3**, summarized in Table S5, reveals that the λ_{max} and absorption wavelength range of these PAs increases and extends with increasing the number of redox centers (**PA1** > **PA3**). **PA1** displays the most red-shifted λ_{max} and comprehensive absorption range than **PA3** (Table S5). Both **PA1** and **PA3** are symmetrical delocalized class III. The results suggest that the polymers containing more electroactive nitrogen centers at the first oxidation stage exhibit a more intensive extended wavelength absorption in the NIR region due to delocalization from a neutral TPA center to other TPA cation radical centers through phenyl bridges in the backbone of the triarylamine-based polymers. Red-shifted wavelength absorption in the NIR region indicates a weak electronic coupling interaction between the different redox states, which might be attributable to the fact that a charge of cation radical could be dispersed or distributed by resonance. Consequently, polymers containing more electroactive nitrogen centers exhibit a longer wavelength absorption in the NIR region, such as **PA1**, **PA1′**, and **PA2**. Thus, the enhanced stability of cation radicals primarily dominates the EC switching stability of TPA-based polymers.

According to the information presented above, two key factors that play crucial roles in affecting the stability of cation radicals are identified. First, the impact of the electron-donating or electron-withdrawing substituents leads to the opposite electrochemical stabilities. The electron-donating substituents adjacent to the phenyl ring attached to the electroactive nitrogen center could effectively stabilize cation radicals, for example, in Scheme 2:

Scheme 2. Substitution Effect of the Functional Groups on the *Para*-Position

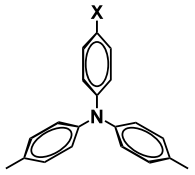

X = OCH_3, CH_3, *t*-Bu [electron-donating group]
NO_2, F, CN [electron-withdrawing group]

Since cation radicals could be considered to be electron-deficient, we would expect an electron-donating group to stabilize cation radicals.

Second, the electrochemical system with a charge of the cation radical dispersed or delocalized by an inductive effect or resonance could facilitate the stabilization effectively. Consequently, the resonance effect of electron delocalization over the electroactive nitrogen centers via phenyl rings contributes to the electrochemical stability. The TPPA cation radical is a symmetrical delocalized class III, and the electron could delocalize over the two redox centers, as shown in Figure 4a.

Thus, polymers **PA1 and PA2** with three electroactive nitrogen centers attached to four phenyl rings were judiciously designed and prepared in this study for elucidating EC behaviors and comparing the EC stability between **PA1**, **PA2**, and TPA-based PA with only two electroactive nitrogen centers attached to three phenyl rings like **PA3**. The results are summarized in Table 1. The methoxy group is an electron-donating substituent because of the contribution of electron density to the phenyl ring through resonance. The chemical structure of **PA1** contains ortho and para two methoxy substituents in the phenyl rings, whereas **PA3** only has one methoxy substituent at the para-position of phenyl rings. The electron-donating effect of substituents on EC stability favors $\mathbf{PA1}^{+\bullet}$ over $\mathbf{PA3}^{+\bullet}$ because **PA1** contains more electron-donating methoxy substituents than **PA3**. Besides, **PA1** with three electroactive nitrogen centers facilitates the formulation of three resonance structures of the resulting cation radical.

Nevertheless, **PA3** with two electroactive nitrogen centers could form only two resonance structures for the corresponding cation radical. More extended resonance structures could contribute to a more effective resonance stabilization in the mix-valence hybrid system, suggesting that the resonance effect of the electron delocalized over the electroactive nitrogen centers on the EC switching stability benefits $\mathbf{PA1}^{+\bullet}$ over that of $\mathbf{PA3}^{+\bullet}$. Accordingly, the electron-donating and resonance effect on the EC stability tends to be $\mathbf{PA1}^{+\bullet}$ over $\mathbf{PA3}^{+\bullet}$, resulting in remarkably higher switching stability for **PA1** than **PA3**. In addition, **PA3** showed a higher EC stability than **PA2**, which might be attributable to the fact that the chemical structure of **PA3** contains methoxy substituents, which are more electron-donating than methyl substituents of **PA2**. Thus, substituent groups with unshared electron pairs on the atom adjacent to the benzene ring, like methoxy, are more vital

https://doi.org/10.1021/acsapm.4c00432
ACS Appl. Polym. Mater. XXXX, XXX, XXX−XXX

electron-releasing groups than groups without unshared electron pairs, like methyl, because the contribution of electron density to the phenyl ring through resonance is generally more substantial than through an inductive effect. Consequently, even though the **PA2**$^{+\bullet}$ cation radical with three electroactive nitrogen centers could form three resonance structures more than **PA3**$^{+\bullet}$ with only two resonance structures from two electroactive nitrogen centers, the electron-donating effect influences more than the resonance effect in this case. Notably, the electrochemical stability for each cation radical center on the TPA-based polymer would be affected by the electron-donating capability of substituents and the resonance delocalization effect over all the electroactive nitrogen centers.

4. CONCLUSIONS

PA1 and **PA2** were judiciously designed and successfully prepared from the synthesized diamine monomers **1-NH$_2$** and **2-NH$_2$** with dicarboxylic acids via a phosphorylation polyamidation rection. **PA1** exhibited exceptional high-performance EC behaviors, including multiple color changes (from colorless to grass green, green, and blue), fast response speed (7.7/2.6 s at 422 nm at the first EC stage), high contrast of optical transmittance change (ΔT% = 54% at 422 nm at the first oxidation stage), and transcendent EC stability. At the first oxidation stage, **PA1** revealed the highest EC stability (only 4.1 and 2.5% decay of CE at 422 and 1252 nm after 15,000 switching cycles, respectively) compared to all other TPA-based reported polymers up to our knowledge. Introducing the electron-donating methoxy substituents to ortho- and para-phenyl positions and three electroactive nitrogen centers attached to four phenyl rings into the core multitriarylamine unit effectively promotes the EC stability of the resulting **PA1**. During the electrochemical oxidation procedures, the color changes of **PA1** and **PA2** are different, indicating that altering the electron-donating substituents attached to the phenyl ring could achieve a color-tuning effect. We noticed the intriguing behavior for the first time that polymers containing more electroactive nitrogen centers could manifest longer wavelength absorption in the NIR region at the first oxidation stage caused by the electron delocalization from a neutral TPA center to the other TPA cation radical center, and this absorption shifting behavior also could bring about an enhanced EC stability. This research distinctly illustrated that incorporating multiple electroactive nitrogen centers into the polymer chain could significantly amplify the EC switching stability of the obtained polymers. Notably, the stability of each cation radical center of the TPA-based polymers depends on both the electron-donating capability from substituents and the resonance effect of the electron delocalization over the electroactive nitrogen centers attached to the bridge of phenyl rings that are demonstrated in this study.

ASSOCIATED CONTENT

Supporting Information

The Supporting Information is available free of charge at https://pubs.acs.org/doi/10.1021/acsapm.4c00432.

^{1}H and ^{13}C NMR spectra, ESI mass spectra, TMA, DMA, electrochemical properties, and single-crystal information (PDF)

AUTHOR INFORMATION

Corresponding Authors

Yaw-Terng Chern − *Department of Chemical Engineering, National Taiwan University of Science and Technology, Taipei 10617, Taiwan*; Email: ytchern@mail.ntust.edu.tw

Guey-Sheng Liou − *Institute of Polymer Science and Engineering, National Taiwan University, Taipei 10617, Taiwan*; orcid.org/0000-0003-3725-3768; Email: gsliou@ntu.edu.tw

Authors

Shu-Juan Zhang − *Department of Chemical Engineering, National Taiwan University of Science and Technology, Taipei 10617, Taiwan*

Shao-Jung Ho − *Department of Chemical Engineering, National Taiwan University of Science and Technology, Taipei 10617, Taiwan*

Yu-Jen Shao − *Institute of Polymer Science and Engineering, National Taiwan University, Taipei 10617, Taiwan*

Yu-Jie Wang − *Institute of Polymer Science and Engineering, National Taiwan University, Taipei 10617, Taiwan*

Complete contact information is available at: https://pubs.acs.org/10.1021/acsapm.4c00432

Notes

The authors declare no competing financial interest.

The crystallographic coordinates for the molecular structure in this study have been deposited at the Cambridge Crystallographic Data Centre (CCDC) under deposition number 2315823 (**1-NO$_2$**). The crystallographic data for **1-NO$_2$** are also available in Tables S6−S10, Supporting Information.

ACKNOWLEDGMENTS

We appreciate the National Science and Technology Council's financial support through Project NSTC 112-2113-M-002−002 and 111-2221-E-002-028 -MY3.

REFERENCES

(1) Monk, P. M. S.; Mortimer, R. J.; Rosseinsky, D. R. *Electrochromism and Electrochromic Devices*; Cambridge University Press: Cambridge, UK, 2007.

(2) Rosseinsky, D. R.; Mortimer, R. J. Electrochromic systems and the prospects for devices. *Adv. Mater.* **2001**, *13* (11), 783−793.

(3) Rai, V.; Singh, R. S.; Blackwood, D. J.; Zhili, D. A review on recent advances in electrochromic devices: a material approach. *Adv. Eng. Mater.* **2020**, *22* (8), No. 2000082.

(4) Wang, Z.; Wang, X.; Cong, S.; Geng, F.; Zhao, Z. Fusing electrochromic technology with other advanced technologies: A new roadmap for future development. *Mater. Sci. Eng. R Rep.* **2020**, *140*, No. 100524.

(5) Niu, J.; Wang, Y.; Zou, X.; Tan, Y.; Jia, C.; Weng, X.; Deng, L. Infrared electrochromic materials, devices and applications. *Appl. Mater. Today.* **2021**, *24*, No. 101073.

(6) Zhai, Y.; Li, J.; Shen, S.; Zhu, Z.; Mao, S.; Xiao, X.; Zhu, C.; Tang, J.; Lu, X.; Chen, J. Recent Advances on Dual-Band Electrochromic Materials and Devices. *Adv. Funct. Mater.* **2022**, *32* (17), No. 2109848.

(7) Dautremont-Smith, W. C. Transition metal oxide electrochromic materials and displays: a review: Part 1: oxides with cathodic coloration. *Display.* **1982**, *3* (1), 3−22.

(8) Feng, F.; Guo, S.; Ma, D.; Wang, J. An overview of electrochromic devices with electrolytes containing viologens. *Sol. Energy Mater. Sol. Cells.* **2023**, *254*, No. 112270.

(9) Huang, Z.-J.; Li, F.; Xie, J.-P.; Mou, H.-R.; Gong, C.-B.; Tang, Q. Electrochromic materials based on tetra-substituted viologen

analogues with broad absorption and good cycling stability. *Sol. Energy Mater. Sol. Cells* **2021**, *223*, No. 110968.
(10) Sönmez, G.; Schwendeman, I.; Schottland, P.; Zong, K.; Reynolds, J. R. N-substituted poly (3, 4-propylenedioxypyrrole) s: high gap and low redox potential switching electroactive and electrochromic polymers. *Macromolecules.* **2003**, *36* (3), 639−647.
(11) Kim, J.; Rémond, M.; Kim, D.; Jang, H.; Kim, E. Electrochromic conjugated polymers for multifunctional smart windows with integrative functionalities. *Adv. Mater. Technol.* **2020**, *5* (6), No. 1900890.
(12) Kim, J.; In, Y. R.; Phan, T. N.-L.; Kim, Y. M.; Ha, J.-W.; Yoon, S. C.; Kim, B. J.; Moon, H. C. Design of Dithienopyran-Based Conjugated Polymers for High-Performance Electrochromic Devices. *Chem. Mater.* **2023**, *35* (2), 792−800.
(13) Souza, V. H.; Schmidt, A.; Zarbin, A. J. A tunable color palette of electrochromic materials achieved through an ingenious stacking of ordinary conducting polymers. *J. Mater. Chem. A* **2023**, *11* (35), 18853−18861.
(14) Yen, H. J.; Liou, G. S. Solution-processable novel near-infrared electrochromic aromatic polyamides based on electroactive tetraphenyl-p-phenylenediamine moieties. *Chem. Mater.* **2009**, *21* (17), 4062−4070.
(15) Liou, G. S.; Lin, H. Y. Synthesis and electrochemical properties of novel aromatic poly (amine− amide) s with anodically highly stable yellow and blue electrochromic behaviors. *Macromolecules.* **2009**, *42* (1), 125−134.
(16) Yen, H. J.; Lin, H. Y.; Liou, G. S. Novel starburst triarylamine-containing electroactive aramids with highly stable electrochromism in near-infrared and visible light regions. *Chem. Mater.* **2011**, *23* (7), 1874−1882.
(17) Yen, H. J.; Liou, G. S. Design and preparation of triphenylamine-based polymeric materials towards emergent optoelectronic applications. *Prog. Polym. Sci.* **2019**, *89*, 250−287.
(18) Wang, B.; Wang, L.; Chen, H.; Jia, Y.; Ma, Y. Electropolymerized Triphenylamine Network Films for High-Performance Transparent to Black Electrochromism and Capacitance. *Adv. Opt. Mater.* **2023**, *11* (4), No. 2201572.
(19) Zhang, W. J.; Lin, X. C.; Li, F.; Huang, Z. J.; Gong, C. B.; Tang, Q. Multicolored electrochromic and electrofluorochromic materials containing triphenylamine and benzoates. *New J. Chem.* **2020**, *44* (38), 16412−16420.
(20) Yu, T.; Theato, P.; Yao, H.; Liu, H.; Di, Y.; Sun, Z.; Guan, S. Colorless electrochromic/electrofluorochromic dual-functional triphenylamine-based polyimides: Effect of a tetraphenylethylene-based π-bridge on optoelectronic properties. *Chem. Eng. J.* **2023**, *451*, No. 138441.
(21) Lv, X.; Li, D.; Ma, Y.; Li, J.; Liu, Y.; Guo, J.; Niu, H.; Zhou, T.; Wang, W. From gas separation to ion transport in the cavity of hyperbranched polyamides based on triptycene aimed for electrochromic and memory devices. *Polym. Chem.* **2022**, *13* (6), 808−818.
(22) Zhang, C.; Zhai, M.; Xia, S.; Fu, X.; Hong, T.; Zhang, B.; Liu, H.; Cai, W.; Niu, H.; Wang, W. Boosting electrochromic properties of polyamides through altering the structure bonded to triarylamine groups by xanthene. *Sol. Energy Mater. Sol. Cells* **2023**, *260*, No. 112497.
(23) Franke, E.; Trimble, C.; Hale, J.; Schubert, M.; Woollam, J. A. Infrared switching electrochromic devices based on tungsten oxide. *J. Appl. Phys.* **2000**, *88* (10), 5777−5784.
(24) Pasquini, C. Near infrared spectroscopy: A mature analytical technique with new perspectives−A review. *Anal. Chim. Acta* **2018**, *1026*, 8−36.
(25) Hao, Q.; Li, Z.-J.; Lu, C.; Sun, B.; Zhong, Y.-W.; Wan, L.-J.; Wang, D. Oriented two-dimensional covalent organic framework films for near-infrared electrochromic application. *J. Am. Chem. Soc.* **2019**, *141* (50), 19831−19838.
(26) Pugliese, M.; Scarfiello, R.; Prontera, C. T.; Giannuzzi, R.; Bianco, G. V.; Bruno, G.; Carallo, S.; Mariano, F.; Maggiore, A.; Carbone, L.; Gigli, G.; Maiorano, V. Visible Light−Near-Infrared Dual-Band Electrochromic Device. *ACS Sustainable Chem. Eng.* **2023**, 9601.
(27) Zeng, J.; Wan, Z.; Li, H.; Liu, P.; Deng, W. Visible and near-infrared electrochromic properties of polymers based on triphenylamine derivatives with acceptor groups. *Sol. Energy Mater. Sol. Cells* **2018**, *178*, 223−233.
(28) Wang, Z.; Gong, W.; Wang, X.; Chen, Z.; Chen, X.; Chen, J.; Sun, H.; Song, G.; Cong, S.; Geng, F. Remarkable near-infrared electrochromism in tungsten oxide driven by interlayer water-induced battery-to-pseudocapacitor transition. *ACS Appl. Mater. Interfaces* **2020**, *12* (30), 33917−33925.
(29) Xia, S.; Gao, Y.; Wang, P.; Ma, Y.; Zhu, D.; Niu, H.; Zhou, T.; Wang, W.; Zhao, X. Three dimensional fluorene-based polyamides facile to transfer ion designed for near-infrared electrochromic application and detection for explosive. *Chem. Eng. J.* **2022**, *437*, No. 135108.
(30) Wang, S.; Todd, E. K.; Birau, M.; Zhang, J.; Wan, X.; Wang, Z. Y. Near-infrared electrochromism in electroactive pentacenediquinone-containing poly (aryl ether) s. *Chem. Mater.* **2005**, *17* (25), 6388−6394.
(31) Beaujuge, P. M.; Reynolds, J. R. Color control in π-conjugated organic polymers for use in electrochromic devices. *Chem. Rev.* **2010**, *110* (1), 268−320.
(32) Thompson, B.; Schottland, P.; Sonmez, G.; Reynolds, J. In situ colorimetric analysis of electrochromic polymer films and devices. *Synth. Met.* **2001**, *119* (1−3), 333−334.
(33) Robin, M. B.; Day, P. Mixed valence chemistry-a survey and classification. *Adv. Inorg. Chem. Radiochem.* **1968**, *10*, 247−422.
(34) Seo, E. T.; Nelson, R. F.; Fritsch, J. M.; Marcoux, L. S.; Leedy, D. W.; Adams, R. N. Anodic oxidation pathways of aromatic amines. Electrochemical and electron paramagnetic resonance studies. *J. Am. Chem. Soc.* **1966**, *88* (15), 3498−3503.
(35) Nelson, R.; Adams, R. Anodic oxidation pathways of substituted triphenylamines. II. Quantitative studies of benzidine formation. *J. Am. Chem. Soc.* **1968**, *90* (15), 3925−3930.
(36) Ito, A.; Ino, H.; Tanaka, K.; Kanemoto, K.; Kato, T. Facile Synthesis, Crystal Structures, and High-Spin Cationic States of All-para-Brominated Oligo (N-phenyl-m-aniline) s. *J. Org. Chem.* **2002**, *67* (2), 491−498.
(37) Hagopian, L.; Koehler, G.; Walter, R. I. Substituent effects on the properties of stable aromatic free radicals. Oxidation-reduction potentials of triaryl-amine-triarylaminium ion systems. *J. Phys. Chem.* **1967**, *71* (7), 2290−2296.
(38) Gu, C.; Jia, A. B.; Zhang, Y. M.; Zhang, S. X. A. Emerging electrochromic materials and devices for future displays. *Chem. Rev.* **2022**, *122* (18), 14679−14721.
(39) Sun, N.; Su, K.; Zhou, Z.; Tian, X.; Jianhua, Z.; Chao, D.; Wang, D.; Lissel, F.; Zhao, X.; Chen, C. High-performance emission/color dual-switchable polymer-bearing pendant tetraphenylethylene (TPE) and triphenylamine (TPA) moieties. *Macromolecules.* **2019**, *52* (14), 5131−5139.
(40) Topal, S.; Ipek, O. S.; Sezer, E.; Ozturk, T. Electrochromic-Hybrid energy storage material consisting of triphenylamine and dithienothiophene. *Chem. Eng. J.* **2022**, *434*, No. 133868.
(41) Różalska, I.; Kułyk, P.; Kulszewicz-Bajer, I. Linear 1, 4-coupled oligoanilines of defined length: preparation and spectroscopic properties. *New J. Chem.* **2004**, *28* (10), 1235−1243.
(42) Hsiao, S. H.; Yang, C. P.; Lin, W. L. Synthesis and characterization of new diphenylfluorene-based aromatic polyamides derived from 9, 9-bis [4-(4-carboxy-phenoxy) phenyl] fluorene. *Macromol. Chem. Phys.* **1999**, *200* (6), 1428−1433.
(43) Yamazaki, N.; Higashi, F.; Kawabata, J. Studies on reactions of the N-phosphonium salts of pyridines. XI. Preparation of polypeptides and polyamides by means of triaryl phosphites in pyridine. *J. Polym. Sci., Polym. Chem. Ed.* **1974**, *12* (9), 2149−2154.
(44) Yamazaki, N.; Matsumoto, M.; Higashi, F. Studies on reactions of the N-phosphonium salts of pyridines. XIV. Wholly aromatic polyamides by the direct polycondensation reaction by using

https://doi.org/10.1021/acsapm.4c00432
ACS Appl. Polym. Mater. XXXX, XXX, XXX−XXX

phosphites in the presence of metal salts. *J. Polym. Sci., Polym. Chem. Ed.* **1975**, *13* (6), 1373−1380.
(45) Ito, A.; Sakamaki, D.; Ichikawa, Y.; Tanaka, K. Spin-delocalization in charged states of para-phenylene-linked dendritic oligoarylamines. *Chem. Mater.* **2011**, *23* (3), 841−850.

https://doi.org/10.1021/acsapm.4c00432
ACS Appl. Polym. Mater. XXXX, XXX, XXX−XXX